coatings

MDPI

Article

Effect of Post-Oxidation Treatment on the Performance and Microstructure of Silicon Carbide Ceramic Membrane

Liqun Hu [1,2,†], Yue Hu [1,2,†], Jiaying Zhu [1,2], Jin Li [1], Pinhua Rao [1], Jian Guo [3], Guanghui Li [1,2,*] and Jinjie Wang [1,2,*]

[1] School of Chemistry and Chemical Engineering, Shanghai University of Engineering Science, Shanghai 201620, China; m040120210@sues.edu.cn (L.H.); huy18805558386@163.com (Y.H.); animate777@163.com (J.Z.); radiant_lj@163.com (J.L.); raopinhua@sues.edu.cn (P.R.)
[2] Innovation Centre for Environment and Resources, Shanghai University of Engineering Science, Shanghai 201620, China
[3] Shandong Silicon Membrane Technology Co., Ltd., Weifang 262517, China; qzsihai@vip.163.com
* Correspondence: 04190004@sues.edu.cn (G.L.); jinjiewang@sues.edu.cn (J.W.); Tel.: +86-137-57261777 (G.L.); +86-21-67791221 (J.W.)
† These authors contributed equally to this work.

Abstract: The post-oxidation treatment (POT) is an important step in the preparation of silicon carbide (SiC) ceramic membranes via recrystallization sintering, which is generally considered to remove any possible free carbon. It is found, however, that increasing the temperature of POT improves not only the hydrophilicity and flux of SiC ceramic membranes but also their mechanical properties, chemical stability, etc. Therefore, it is necessary to study the principle of POT in order to obtain SiC ceramic membranes with optimal properties. In this study, the principle of POT was characterized via scanning electron microscopy, X-ray diffraction, X-ray photoelectron spectroscopy, synchronous thermal analysis, and metallographic microscopy. According to the principle, the conditions, such as the temperature and air flow rate, of the post-oxidation process were optimized. Under the optimized conditions, POT improved the flux of SiC ceramic membranes from 1074 to 5118 $L \cdot m^{-2} \cdot h^{-1} \cdot bar^{-1}$, increased the bending strength from 26 to 35 MPa, and provided SiC ceramic membranes with high stability under acid and alkali conditions.

Keywords: silicon carbide; oxidation; porous materials; membrane performance

Citation: Hu, L.; Hu, Y.; Zhu, J.; Li, J.; Rao, P.; Guo, J.; Li, G.; Wang, J. Effect of Post-Oxidation Treatment on the Performance and Microstructure of Silicon Carbide Ceramic Membrane. *Coatings* **2023**, *13*, 957. https://doi.org/10.3390/coatings13050957

Academic Editor: Günter Motz

Received: 20 April 2023
Revised: 15 May 2023
Accepted: 17 May 2023
Published: 19 May 2023

1. Introduction

Ceramic membranes have gained constant attention in both academic research and industry, due to their excellent chemical, thermal, and mechanical performances [1]. They have been widely used in water treatments and material separation [2–4]. Typical ceramic membranes include alumina (Al_2O_3), silicon nitride (Si_3N_4), zirconia (ZrO_2), titania (TiO_2), and silicon carbide (SiC) [5–9]. Due to their high corrosion resistance, high-temperature resistance, and good hydrophilicity, SiC ceramic membranes have become one of the best solutions in oily wastewater, acidic and alkali wastewater, and caustic liquid treatments [10–13].

The crystal structure and high covalent bonding performance of the Si–C bond provide SiC with many excellent properties [14–16]. Meanwhile, the strong covalent bonding and low diffusion coefficient also make SiC membrane preparation difficult [17,18]. The preparation methods of SiC ceramic membranes reported in the literature include particle packing [19], reaction sintering [20], polymer cracking [21], and chemical vapor deposition [22–24]. The particle packing approach, based on the recrystallization sintering process, is often used in the commercial production of SiC ceramic membranes [25]. The preparation of SiC ceramic membranes via recrystallization sintering usually consists of preparing a powder slurry, extrusion molding, high-heat sintering, and post-oxidation treatment (POT) [26–28].

Many studies on SiC membrane preparation using the high-temperature recrystallization method have been reported, encompassing the sintering temperature, membrane

pore size control, mechanical strength, and sintering additives [19,21,29,30]. Comparatively, even though POT is widely applied by the scientific community and industries, there are only a few published works about it. Generally, the oxidation temperature of POT is 450–800 °C to remove the residual carbon [12,27,31–34]. Eray et al. [12] prepared pure silicon carbide membranes on a macroporous SiC support via ceramic processing. During the preparation, the membranes after sintering were passivated in a surface oxidation step in air below 800 °C. This treatment removed the free carbon that eventually formed in the pores, except that some smoothing of the surface roughness did not cause a significant difference in the surface morphology. Ojalvo et al. [27] prepared B_4C ultrafiltration membranes on SiC supporting layers via sintering and calcination. In the experiment, the temperature of POT was 450 °C, which was applicable to cleansing the membranes of possible free carbon, with hardly any B_4C oxidation.

It is found, however, that the surface properties of SiC membranes, such as the surface hydrophilicity, are strongly influenced by POT. Besides the oxidation temperature, the oxidation time and the oxidation environment are also key factors in POT. Therefore, this study aims to deepen some still unknown aspects of POT in terms of mechanisms and process parameters. In this paper, the key factors and optimized conditions of POT are explored. The mechanism of POT is discussed. The effect of POT on membrane performance is investigated. For this, scanning electron microscopy (SEM), X-ray diffraction (XRD), X-ray photoelectron spectroscopy (XPS), synchronous thermal analysis (TGA-DSC), metallographic microscopy (MM), and other characterization methods were used in this work. Based on the results of the current study, a SiC ceramic membrane with excellent performance was prepared.

2. Experimental Procedures

2.1. Raw Materials

The multichannel SiC ceramic membrane after recrystallization was an unoxidized membrane, and the contrast membrane was a membrane after high-temperature oxidation treatment. The unoxidized SiC ceramic membrane was provided by Shandong Silicon Membrane Technology Co., Ltd. (Weifang, China). The size of the membranes was 50 cm × 15 cm × 0.55 cm.

According to the supplier's information, the preparation of the SiC ceramic membrane was divided into two steps: the preparation of the support and the selective layer. First, coarse SiC particles were mixed with hydroxypropyl methyl cellulose and water, then extruded into a multichannel shape, and finally recrystallized in a graphite furnace above 2000 °C to obtain the support. Second, fine SiC particles, hydroxypropyl methyl cellulose, water, and dispersant were mixed with milling balls in a certain proportion. The balls used here were made of zirconium oxide. After defoaming, under the joint action of the air compressor and spraying machine, the SiC slurry was evenly sprayed on the surface of the support to produce a green body. After the body was dried, it was placed into a graphite furnace for high-temperature recrystallization, which produced an unoxidized membrane. The last step was POT, where the SiC ceramic membrane was calcined with air in a muffle or tube furnace at high temperatures.

2.2. Preparation of SiC Ceramic Membrane

The unoxidized SiC membrane from Shandong Silicon Membrane Technology Co., Ltd. was cut into a size of 11 cm × 3.5 cm using a manual fast cutting instrument (SYJ-200H, Shenyang Kejing Automation Equipment Co., Ltd., Shenyang, China). The membrane was cleaned with water and ethanol using ultrasonic cleaning instruments (Kunshan KQ-100, Kunshan Ultrasonic Instrument Co., Ltd., Kunshan, China) for 5 min and then dried for later use.

2.3. Post-Oxidation Treatment

POT mainly involves several parameters: oxidation temperature, time, and air flow rate. A muffle furnace (Hefei KSL-1400X-A1, Hefei Kejing Material Technology Co., Ltd.,

Hefei, China) and tube furnace (Hefei KSL-1700X-A1, Hefei Kejing Material Technology Co., Ltd., Hefei, China) were used to investigate the effect of the oxidation environments. The oxidation temperature was 500 to 1000 °C; the residence time was optimized at 15, 30, and 60 min; and the air flow rate was 0, 80, and 250 mL/min. Both heating procedures heated up at 5 °C/min until the target temperature was reached, which was held for a period of time, and finally cooled down naturally. The main difference between the two heating methods was the difference in the air flow rate during heating. It was assumed that the muffle furnace's air flow rate was 0 mL/min. The oxidized membrane prepared in the muffle furnace was used to compare the properties and explore the temperature, holding time, and oxidation principle. Then, the effect of the air flow rate was investigated using a tube furnace.

2.4. Characterization Techniques

The changes in SiC ceramic membranes before and after POT were characterized using a variety of analytical methods.

A contact angle measurement instrument (SDC-200S, Dongguan Shengding Precision Instrument Co., Ltd., Dongguan, China) was used to measure the water contact angle (WCA) of the ceramic membrane. Additionally, the measurement medium was RO water. The measurement of the contact angle referred to the national standard (GB/T 30693-2014). Five test points were selected on the membrane surface, and the average value was calculated as the contact angle of the sample. The contact angle of each test point was the average contact angle at the time of 0 s and 1 s when the water droplet contacted the membrane surface. For the measurement of the underwater oil contact angle (OCA), it was necessary to measure the contact angle after the underwater oil droplets remained on the surface of the selective layer for 2 s.

The four-point bending method was used to measure the effect of POT on the mechanical strength of the membranes. Three samples were tested to obtain the average strength. The zeta potential of the SiC ceramic membrane selective layer powder was measured using a Malvern Zetasizer (Nano S900, Malvern Instruments Ltd., Malvern, UK) to explore the effect of the POT temperature on its zeta potential.

The pure water flux of the SiC membrane was measured using a membrane flux measurement instrument in the laboratory. The calculation equations are as follows:

$$J = V/(S \cdot t \cdot P) \tag{1}$$

where J, s, t, and P represent the penetration flux of pure water ($L \cdot m^{-2} \cdot h^{-1} \cdot bar^{-1}$), membrane test area ($m^2$), test time (h), and test pressure (bar), respectively.

The SiC ceramic membrane's rejection rate of polystyrene (PS) nanoparticles (300 nm and 500 nm) was measured using a self-made filtration device. The calculation method is as follows:

$$R = (1 - C_t / C_0) \times 100\% \tag{2}$$

where R is the rejection rate (%), and C_0 and C_t are the concentrations of PS nanoparticles in the feeding and permeate solutions, respectively.

The method for detecting the chemical stability of the SiC ceramic membrane was as follows: At room temperature, the unoxidized and post-oxidized samples were immersed in sulfuric acid (H_2SO_4) solutions (0.1 mol/L) and sodium hydroxide (NaOH) solutions (0.1 mol/L) for 60 days. The weight loss and corrosion appearance of the membrane before and after soaking due to corrosion were evaluated. The weight loss was calculated according to the following equation:

$$\Delta W = (W_{uc} - W_c)/W_{uc} \times 100\% \tag{3}$$

where ΔW is the weight loss ratio (%), and W_{uc} and W_c are the weights (g) of the membrane sample before and after corrosion testing, respectively.

Additionally, various detection methods were used to discuss the principle of POT. SEM (SU8010, Anqi Technology Co., Ltd., Shanghai, China) was used to observe the surface morphology of the membrane. The crystal changes in the membrane were observed using MM (WMJ-9688, Shanghai Wumo Optical Instrument Co., Ltd., Shanghai, China). An XRD analyzer (Nishiko rigaku Ultima IV, Beijing Guanyuan Technology Co., Ltd., Beijing, China) was used to analyze the phase change of the membrane surface, and XPS was used to analyze the elements of the membrane. The weight change of the SiC membrane during the sintering process was measured using a synchronous thermal analyzer (TA Q600, Shenzhen Huapu General Technology Co., Ltd., Shenzhen, China).

3. Results and Discussion

3.1. Effect of POT on the Properties of SiC Membrane

In the existing literature, the post-oxidation process temperature in the preparation of SiC ceramic membranes is usually 450–800 °C to remove the residual free carbon in the material [12,27,31–34].

However, our study found that when the temperature of the post-oxidation process increased (such as 900 °C), the ceramic membrane obtained a better performance than the membrane without oxidation and the membrane oxidized at 500 °C. A comparison of the appearance, surface hydrophilicity, pure water flux, mechanical properties, and chemical stability of the three SiC membranes is shown below.

During the preparation of the SiC ceramic membrane, the color of the membrane changed in each treatment stage. Figure 1 shows photographs of the unoxidized membrane and the membranes post-oxidized at 500 and 900 °C. It can be seen that the color of the unoxidized membrane was similar to that of the membrane oxidized at 500 °C. However, when the temperature increased to 900 °C, the color of the surface gradually turned cyan.

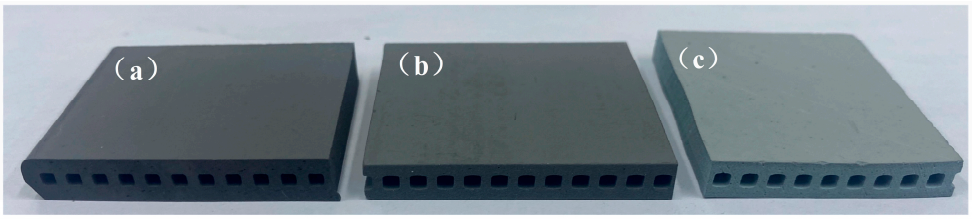

Figure 1. Photographs of the SiC membrane: (**a**) the unoxidized SiC membrane, (**b**) the SiC membrane post-oxidized at 500 °C, and (**c**) the SiC membrane post-oxidized at 900 °C.

WCA is normally used to evaluate the hydrophilicity of membranes. The smaller the WCA, the higher the membrane hydrophilicity [35]. Figure 2 compares photographs of the three membranes at 0 s in the contact angle test (the shooting speed of the water contact angle was 50 ms/frame). Obviously, the contact angle of the unoxidized membrane was very large, but after POT, it sharply decreased. The post-oxidation process increased the hydrophilic property of the SiC membrane.

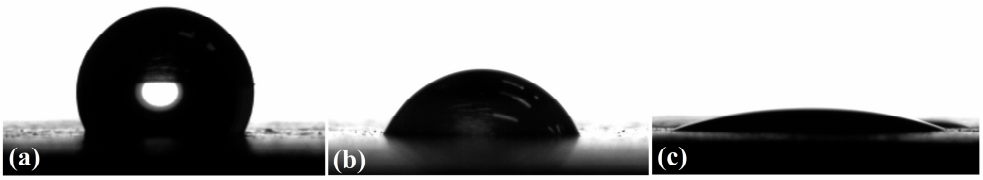

Figure 2. Measurement results of WCA: (**a**) the unoxidized SiC membrane, (**b**) the SiC membrane post-oxidized at 500 °C, and (**c**) the SiC membrane post-oxidized at 900 °C.

A membrane's hydrophilicity is closely related to its flux. Table 1 shows the water permeate flux of the unoxidized membrane and the membranes oxidized at 500 °C and 900 °C. The results show that the permeate flux increased with increasing POT temperature.

There was little difference in flux between the unoxidized membrane and the membrane post-oxidized at 500 °C. The increase in flux was the most obvious when the POT temperature rose to 900 °C. In addition, the mechanical property of SiC was also affected by POT. As shown in Table 1, the mechanical property (bending strength) of the post-oxidized SiC membranes was higher than that of the unoxidized membrane.

Table 1. Properties of the unoxidized membrane and the membranes post-oxidized at 500 °C and 900 °C.

SiC Membranes	Unoxidized	Post-Oxidized at 500 °C	Post-Oxidized at 900 °C
WCA/°	116.0 ± 7.9	64.6 ± 6.2	9.0 ± 1.5
Permeate flux/($L \cdot m^{-2} \cdot h^{-1} \cdot bar^{-1}$)	1074 ± 22	1175 ± 51	4330 ± 297
Bending strength/MPa	26 ± 3	28 ± 2	35 ± 8
Weight loss rate (0.1 mol/L H_2SO_4)/%	−0.30	−0.26	−0.36
Weight loss rate (0.1 mol/L NaOH)/%	0.08	0.05	0.25

To compare the chemical stability of the SiC membrane before and after oxidation, the membranes were cut into uniform blocks and exposed to strong acid and alkali solutions at room temperature for 60 days. Due to the excellent chemical stability of SiC, the weight change of the SiC membranes treated at different temperatures in acid and alkali solutions did not exceed 0.4%, as shown in Table 1.

Figure 3 shows the surface morphology of the SiC membranes before and after being corroded in acid and alkali solutions for 60 days. The surface of the unoxidized membrane soaked in acid and alkali solutions was corroded, and the corrosion in the strong alkali solution was the most serious (Figure 3a). Compared to the unoxidized membrane, the surface of the membrane post-oxidized at 900 °C was intact and almost corrosion-free. The post-oxidized ceramic membrane presented good corrosion resistance in the long-term experiments (Figure 3b). The results of this test show that this post-oxidized membrane has high stability under acidic and alkaline conditions.

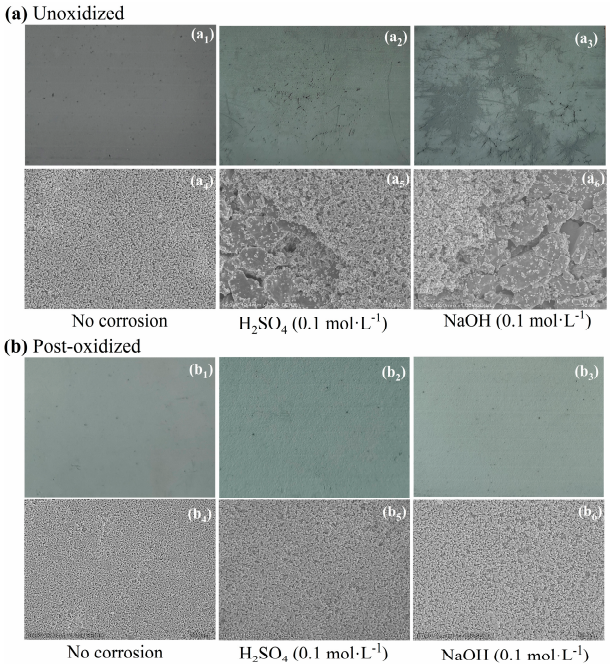

Figure 3. Surface morphology of (**a**) unoxidized and (**b**) post-oxidized SiC ceramic membranes after 60 days of no corrosion, acid corrosion, and base corrosion: (**a1**–**a3**) are surface photographs (top of (**a**)); (**a4**–**a6**) are SEM images (bottom of (**a**)); (**b1**–**b3**) are surface photographs (top of (**b**)); (**b4**–**b6**) are SEM images (bottom of (**b**)).

3.2. Principle of POT

In order to explore the principle of the mechanism of POT, the XRD, XPS, SEM, MM, and TG characterization methods were used to characterize the membrane under different conditions. The post-oxidized membrane refers to the membrane oxidized at 900 °C in the muffle furnace.

Firstly, the SiC ceramic membrane was analyzed using X-ray diffraction to observe any changes in its composition before and after post-oxidation. According to the XRD spectrum (Figure 4a), both the unoxidized and post-oxidized membranes were mainly 6H–SiC. Figure 4b is an enlargement of the ordinate in Figure 4a, from which it can be seen that C and ZrC were present in the unoxidized membrane. After POT, the peaks of C and ZrC disappeared and were replaced by the peaks of ZrO_2.

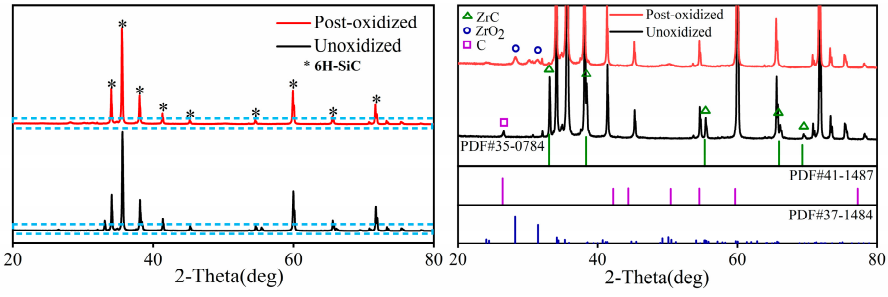

(**a**) (**b**)

Figure 4. The XRD patterns of (**a**) the unoxidized and post-oxidized SiC ceramic membranes; (**b**) an enlargement of the ordinate in (**a**).

Figure 5 shows the XPS spectra of the SiC ceramic membrane before and after POT. According to the full XPS spectrum (Figure 5a), the peak of C1s became weaker and the absorption peaks of O1s, Si2p, and Zr3d increased after POT. Concerning the Si2p region (Figure 5b), the unoxidized sample had one peak at 100.2 eV, corresponding to SiC. The peak at 100.2 eV of the post-oxidized sample became weaker, while one new peak appeared at 103.2 eV, corresponding to SiO_2, which was oxidized during POT [36]. This can also be confirmed by the O1s region (Figure 5d), where the SiO_2 (532.3 eV [33]) component of the post-oxidized sample is much higher than that of the unoxidized sample.

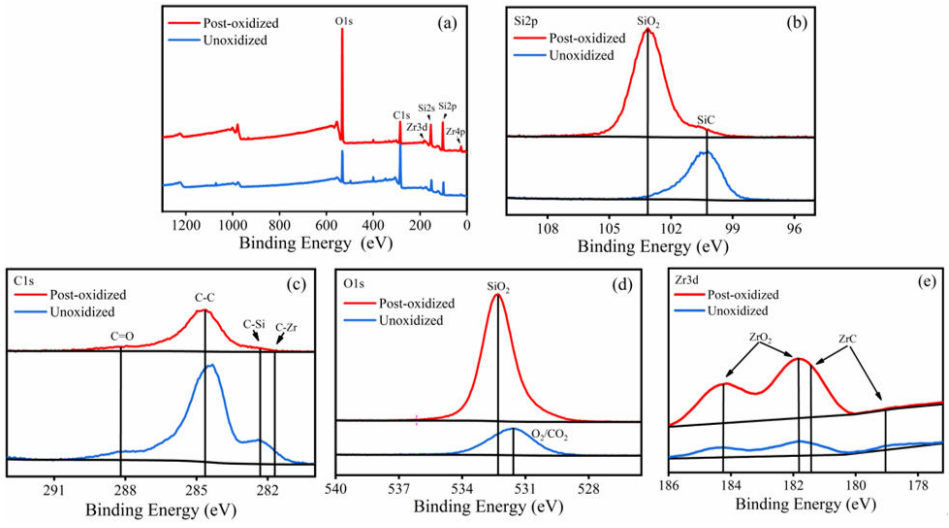

Figure 5. XPS spectra of the unoxidized and post-oxidized SiC ceramic membranes: (**a**) full spectrum, (**b**) Si2p, (**c**) C1s, (**d**) O1s, and (**e**) Zr3d.

The C1s spectrum deconvoluted into peaks at 288.3, 284.5, 282.5, and 281.4 eV, corresponding to C=O, C–C, C–Si, and C–Zr bonds, respectively [37,38]. The carbon component of the post-oxidized sample was significantly lower than that of the unoxidized sample, indicating the disappearance of the carbon element. In Figure 5e, the two peaks at 182.1 and 184.5 eV were attributed to $3d_{5/2}$ and $3d_{3/2}$ of ZrO_2; moreover, the two peaks at 179.12 and 181.44 eV were attributed to ZrC. XPS analysis suggested that POT resulted in the disappearance of free carbon, and the formation of SiO_2 and ZrO_2 in the selective layer of the SiC membrane.

Figure 6 shows the surface morphology and polarization phenomenon of the SiC ceramic membrane before and after oxidation. Many fine impurities can be seen on the surface of the unoxidized membrane, as shown in Figure 6a. After POT, the tiny impurities on the membrane surface disappeared. Combined with the previous XRD and XPS characterizations, these impurities were determined to be carbon residues. The carbon residues were oxidized out during POT and more of the SiC surface became exposed. The SiC surface had a large number of hydroxyl groups. This is the reason why the hydrophilicity of SiC was significantly enhanced by POT [39]. Figure 6c,d show the polarization phenomenon of the SiC membrane oxidized at 900 °C using MM with different polarization angles. It can be seen from the microscope images that when the polarization angle changed from 354° to 200°, small amounts of crystals on the surface of the post-oxidized membrane turned from entirely black to light-emitting, as found for the ZrO_2 pellets. The results show that the surface of the post-oxidized membrane contained ZrO_2.

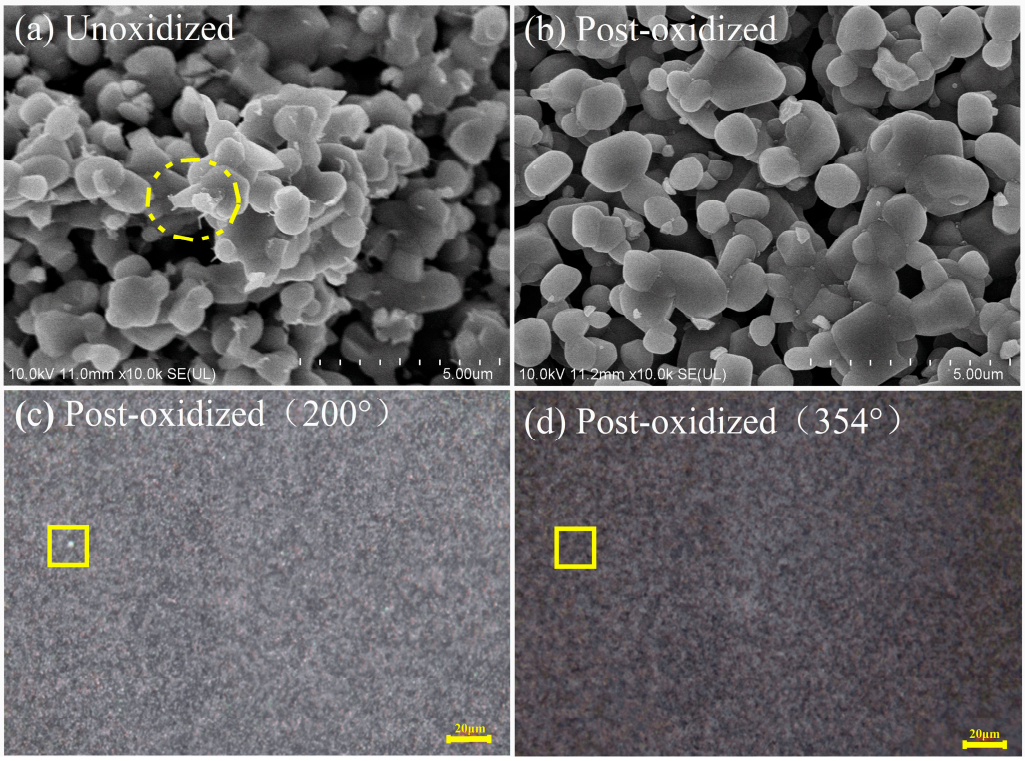

Figure 6. Comparison of the SEM images between (**a**) the unoxidized membrane and (**b**) the post-oxidized membrane; the polarization phenomenon of the surface of the post-oxidized SiC ceramic membrane at different polarization angles: (**c**) 200° and (**d**) 354°.

The TGA-DSC curve of the unoxidized membrane after heat treatment at 20–800 °C is shown in Figure 7. According to the TG curve, the unoxidized membrane was in a state of weight loss during the initial heat treatment process, and the weight increased when the temperature reached 500 °C. Meanwhile, according to the DSC curve, there were two distinct exothermic peaks around 350 °C and 600 °C, which implies that at least

two chemical reactions occurred in the POT. Based on the literature, these two chemical reactions were considered to be the oxidation of free carbon to CO_2/CO and that of ZrC to ZrO_2 [40,41].

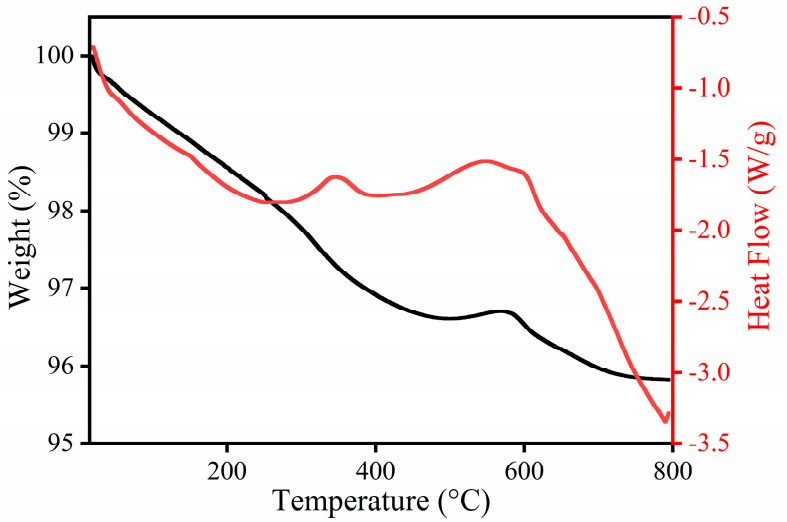

Figure 7. TGA-DSC curve of the unoxidized membrane heated in air at a heating rate of 10 °C/min.

The weight loss ratios of the SiC membrane samples were measured after POT at different temperatures, as shown in Table 2. From 700 °C, the weight loss ratio increased relatively significantly, indicating that ZrC had been wholly oxidized to ZrO_2, but carbon was still consumed in this process. When the post-oxidation temperature rose to 800 °C, the weight loss ratio began to increase again, which means that a third chemical reaction occurred. Amorphous SiO_2 was reported to form when the temperature of SiC in air reached more than 800 °C [42].

Table 2. Weight loss ratios of the SiC membrane samples after POT at different temperatures.

Temperature/°C	500	600	700	800	900	1000
Weight loss ratio/%	−0.06	0.03	1.17	1.09	1.11	0.03

These results suggested that the SiC membrane after recrystallization contained C and ZrC. The free C came from the decomposition of organic additives at high temperatures. Additionally, Zr came from the zirconia ball used in the ball grinding process for the preparation of the membrane slurry. After POT, the C on the surface of the SiC ceramic membrane gradually disappeared, while the silicon hydroxyl groups increased. Finally, a small amount of ZrC in the membrane was transformed into ZrO_2. The presence of Zr has a certain impact on the chemicals in the SiC ceramic membrane. However, this effect can be eliminated by replacing the grinding ball. In addition, silica is formed when the post-oxidation temperature reaches 800 °C. The chemical changes that may be involved in the post-oxidation process of SiC ceramic membrane preparation are as follows [41,43]:

$$C(s) + O_2(g) \rightarrow CO_2(g) \quad (4)$$

$$C(s) + 1/2O_2(g) \rightarrow CO(g) \quad (5)$$

$$ZrC(s) + 2O_2(g) \rightarrow ZrO_2(s) + CO_2(g) \quad (6)$$

$$ZrC(s) + 3/2O_2(g) \rightarrow ZrO_2(s) + CO(g) \quad (7)$$

$$SiC(s) + 2O_2(g) \rightarrow SiO_2(s) + CO_2(g) \quad (8)$$

$$SiC(s) + 3/2O_2(g) \rightarrow SiO_2(s) + CO(g) \quad (9)$$

3.3. Optimization of POT

POT can significantly improve the performance of SiC membranes, including flux, mechanical strength, and chemical resistance. Therefore, it is necessary to study and optimize the oxidation conditions, such as the oxidation temperature, oxidation time, and air flow rate.

Table 3 lists the WCA, underwater OCA, permeate flux, bending strength, and zeta potential of the SiC membrane samples after the oxidation treatment at different temperatures using a muffle furnace. The WCAs were strongly dependent on the oxidation temperatures. The higher the oxidation temperatures, the lower the WCA values. Moreover, the pure water flux was closely related to the WCA. The flux of the sample oxidized at 900 °C was more than triple that of the sample oxidized at 500 °C. The underwater OCA was the largest at 800–900 °C. The large underwater OCA indicates that this POT-treated SiC ceramic membrane has good application prospects for oil–water separation. The mechanical strength of the SiC membrane was also obviously affected by the oxidation temperature. However, POT had little effect on the zeta potential of the SiC ceramic membrane. Based on the performance improvement and the cost control, the POT temperature is recommended to be 800–900 °C when using a muffle furnace.

Table 3. Changes in the properties of the post-oxidized SiC membrane at different temperatures.

Temperature/°C	500	700	800	900	1000
WCA/°	64.6 ± 6.2	11.2 ± 3.2	10.1 ± 1.7	9.0 ± 1.5	12.4 ± 1.7
Underwater OCA/°	146.6 ± 5.3	160.6 ± 1.0	162.4 ± 3.3	162.2 ± 1.5	156.3 ± 1.9
Permeate flux/L·m^{-2}·h^{-1}·bar^{-1}	1175 ± 51	4134 ± 278	4326 ± 251	4330 ± 297	4400 ± 275
Bending strength/MPa	28 ± 2	28 ± 3	38 ± 3	35 ± 8	35 ± 4
Zeta potential/mV	−24.6 ± 0.5	−22.8 ± 0.9	−25.0 ± 0.1	−24.4 ± 0.6	−22.0 ± 0.7

The oxidation time was optimized at the post-oxidation temperature of 900 °C and was set to 15, 30, and 60 min. The results of the corresponding WCAs, permeate fluxes, and rejection rates of PS nanoparticles are shown in Table 4. The difference in the WCA under different oxidation times was not obvious. In contrast, the effect of 30 min of residence was relatively better. The permeate flux reached the maximum when the oxidation time was 30 min, while the retention rate of 300 nm PS nanoparticles reached the maximum when the oxidation time was 60 min. In view of maintaining a good permeate flux and retention, 30 min was selected as the oxidation time of the POT.

Table 4. The WCAs of the SiC membrane at different oxidation times.

SiC Membrane	Oxidized at 900 °C in a Muffle Furnace		
Time/min	15	30	60
WCA/°	11.0 ± 0.5	9.0 ± 1.5	10.3 ± 1.6
Permeate flux/L·m^{-2}·h^{-1}·bar^{-1}	4072 ± 193	4330 ± 297	3685 ± 174
Rejection rates (300 nm)/%	61.08% ± 0.01	61.71% ± 0.00	77.83% ± 0.04
Rejection rates (500 nm)/%	98.62% ± 0.00	98.90% ± 0.00	99.04% ± 0.00

Optimization of the conditions at different air flow rates was achieved mainly by using muffle and tube furnaces. There was no air control when using the muffle furnace. Compared with the tube furnace, the gas flow rate in the muffle furnace was assumed to be 0 mL/min. The WCAs, permeate fluxes, and rejection rates of the post-oxidized membrane at different temperatures with different air flow rates are shown in Figure 8.

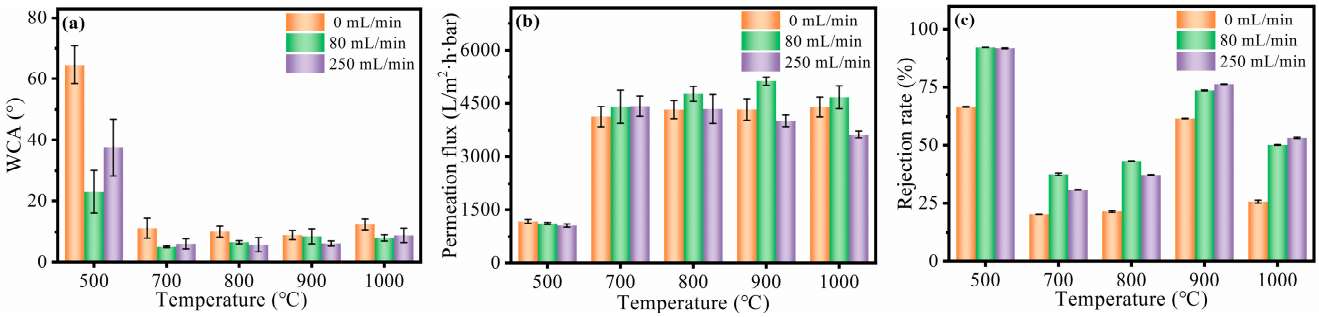

Figure 8. The (**a**) WCAs, (**b**) permeate fluxes, and (**c**) rejection rates of the 300 nm fluorescent probe of the post-oxidized membrane at different temperatures under different air flow rates.

As shown in Figure 8a, the value of the WCA dropped sharply when the post-oxidation temperature was higher than 700 °C. Additionally, the samples treated in the tube furnace had lower WCAs than those treated in the muffle furnace, which can also be found from the measurement of the permeate flux (Figure 8b). At the air flow rate of 80 mL/min, the permeate flux of the post-oxidized membrane was higher than that under the other air flow rates, especially at 900 °C. This was mainly because of the insufficient air supply in the muffle furnace. When the air is in a static state, it cannot timely supplement the consumed oxygen, which makes the oxidation insufficient. The rejection of PS nanoparticles by the membrane was also examined. Both 300 nm and 500 nm PS nanoparticles were used as detection probes. The rejections of the 500 nm nanoparticles were more than 99% for all samples, while the rejections of the 300 nm PS nanoparticles were temperature-dependent (Figure 8c). Although the membrane treated with POT at 500 °C had the highest rejection of 300 nm spheres, the flux of the membrane was very low. Therefore, 500 °C was not a good choice. Relatively, 900 °C was a more suitable choice. The membrane treated at this temperature had a higher flux and retention. This may be due to the fact that the pore size of the ceramic membrane was reduced by the SiO_2 produced by the slight oxidation of SiC at 900 °C. Additionally, excessive oxidation may cause damage to the selective layer of the membrane when the post-oxidation temperature is 1000 °C [44]. Based on the experimental results and analysis, the optimized conditions of POT were an operating temperature of 900 °C, an oxidation time of 30 min, and an air flow rate of 80 mL/min.

As listed in Table 5, the POT-treated SiC ceramic membrane exhibited superior performances, particularly in terms of its membrane permeability, compared to those of other ceramic membranes. Thus, this POT-treated SiC ceramic membrane has good application prospects.

Table 5. Comparison of the permeate flux and strength with those of other ceramic membranes.

Material	Pore Size/μm	Permeate Flux /L·m^{-2}·h^{-1}·bar^{-1}	Strength/MPa	Ref.
SiO_2–Si_3N_4	0.52	1080	200	[45]
SiC (Without POT)	0.87	2140	25	[46]
ZrO_2–SiC	0.082	850	38	[46]
TiO_2–Al_2O_3	0.65	1500	–	[47]
Al_2O_3	0.76	8	–	[48]
SiC	0.50	4330	35	This work

4. Conclusions

In this paper, using the XRD, XPS, SEM, and MM characterization methods, we comprehensively studied the POT of SiC ceramic membranes. In the POT, the carbon loaded on the membrane surface disappeared. At the same time, a slight oxidation reaction occurred on the surface of SiC to produce SiO_2. The removal of carbon on the membrane surface and the presence of trace SiO_2 led to a better hydrophilicity and higher flux of the membrane, and improved mechanical properties. By optimizing the conditions of the

process parameters, 900 °C for 30 min with an air flow rate of 80 mL/min was the best process condition. The SiC membrane prepared under the optimal conditions has not only good hydrophilicity and chemical stability, but also a good permeate flux and bending strength, and even its retention performance can be improved. This study is significant for the production of SiC ceramic membranes.

Author Contributions: Conceptualization, J.W.; formal analysis, Y.H. and J.Z.; investigation, Y.H. and J.L.; methodology, L.H.; resources, J.G.; software, P.R.; supervision, G.L. and J.W.; validation, L.H.; writing—original draft, L.H. and Y.H.; writing—review and editing, P.R., G.L. and J.W. All authors have read and agreed to the published version of the manuscript.

Funding: This research was funded by the Capacity Building Project of Some Local Colleges and Universities in Shanghai (No. 21010501400) and National Natural Science Foundation of China (Grant 21806103).

Institutional Review Board Statement: Not applicable.

Informed Consent Statement: Not applicable.

Data Availability Statement: Not applicable.

Conflicts of Interest: The authors declare no conflict of interest.

References

1. Li, C.; Sun, W.; Lu, Z.; Ao, X.; Li, S. Ceramic nanocomposite membranes and membrane fouling: A review. *Water Res.* **2020**, *175*, 115674. [CrossRef] [PubMed]
2. Nasir, A.M.; Adam, M.R.; Kamal, S.N.E.A.M.; Jaafar, J.; Othman, M.H.D.; Ismail, A.F.; Aziz, F.; Yusof, N.; Bilad, M.R.; Mohamud, R.; et al. A review of the potential of conventional and advanced membrane technology in the removal of pathogens from wastewater. *Sep. Purif. Technol.* **2022**, *286*, 120454. [CrossRef] [PubMed]
3. Othman, N.H.; Alias, N.H.; Fuzil, N.S.; Marpani, F.; Shahruddin, M.Z.; Chew, C.M.; Ng, K.M.D.; Lau, W.J.; Ismail, A.F. A Review on the Use of Membrane Technology Systems in Developing Countries. *Membranes* **2021**, *12*, 30. [CrossRef] [PubMed]
4. Scholes, C.A. Pilot plants of membrane technology in industry: Challenges and key learnings. *Front. Chem. Sci. Eng.* **2020**, *14*, 305–316. [CrossRef]
5. Sinhamahapatra, S.; Dana, K.; Tripathi, H.S. Enhancement of reaction-sintering of alumina-excess magnesium aluminate spinel in presence of titania. *Ceram. Int.* **2018**, *44*, 10773–10780. [CrossRef]
6. Luo, C.; Zhang, Y.; Deng, T. Pressureless sintering of high performance silicon nitride ceramics at 1620 °C. *Ceram. Int.* **2021**, *47*, 29371–29378. [CrossRef]
7. Pang, X.; Xi, C.; Wang, T. Phase stability (at 1000 °C) of hollow t-ZrO_2 fibers costabilized by lanthana and yttria. *Int. J. Appl. Ceram. Technol.* **2020**, *17*, 1646–1651. [CrossRef]
8. Li, X.; Yao, D.; Zuo, K.; Xia, Y.; Yin, J.; Liang, H.; Zeng, Y.-P. Fabrication, microstructural characterization and gas permeability behavior of porous silicon nitride ceramics with controllable pore structures. *J. Eur. Ceram. Soc.* **2019**, *39*, 2855–2861. [CrossRef]
9. Cao, J.; Lu, Z.; Miao, K.; Zhao, H.; Xia, Y.; Wang, F.; Lu, B. Fabrication of high-strength porous SiC-based composites with unidirectional channels. *J. Am. Ceram. Soc.* **2019**, *102*, 4888–4898. [CrossRef]
10. Jiang, Q.; Wang, Y.; Xie, Y.; Zhou, M.; Gu, Q.; Zhong, Z.; Xing, W. Silicon carbide microfiltration membranes for oil-water separation: Pore structure-dependent wettability matters. *Water Res.* **2022**, *216*, 118270. [CrossRef]
11. Bessa, L.P.; Ferreira, E.D.P.; Cardoso, V.L.; Reis, M.H.M. Air-sintered silicon (Si)-bonded silicon carbide (SiC) hollow fiber membranes for oil/water separation. *J. Eur. Ceram. Soc.* **2021**, *42*, 402–411. [CrossRef]
12. Eray, E.; Boffa, V.; Jørgensen, M.K.; Magnacca, G.; Candelario, V.M. Enhanced fabrication of silicon carbide membranes for wastewater treatment: From laboratory to industrial scale. *J. Membrane Sci.* **2020**, *606*, 118080. [CrossRef]
13. Li, R.; Kadrispahic, H.; Jørgensen, M.K.; Berg, S.B.; Thornberg, D.; Mielczarek, A.T.; Bester, K. Removal of micropollutants in a ceramic membrane bioreactor for the post-treatment of municipal wastewater. *Chem. Eng. J.* **2022**, *427*, 131458. [CrossRef]
14. Kim, S.C.; Kim, Y.-W.; Song, I.-H. Processing and properties of glass-bonded silicon carbide membrane supports. *J. Eur. Ceram. Soc.* **2017**, *37*, 1225–1232. [CrossRef]
15. Shcherban, N.D. Review on synthesis, structure, physical and chemical properties and functional characteristics of porous silicon carbide. *J. Ind. Eng. Chem.* **2017**, *50*, 15–28. [CrossRef]
16. Bukhari, S.Z.A.; Ha, J.-H.; Lee, J.; Song, I.-H. Fabrication and optimization of a clay-bonded SiC flat tubular membrane support for microfiltration applications. *Ceram. Int.* **2017**, *43*, 7736–7742. [CrossRef]
17. Margiotta, J.C.; Zhang, D.J.; Nagle, D.C. Microstructural evolution during silicon carbide (SiC) formation by liquid silicon infiltration using optical microscopy. *Int. J. Refract. Met. Hard Mater.* **2010**, *28*, 191–197. [CrossRef]
18. Bukhari, S.Z.A.; Ha, J.-H.; Lee, J.; Song, I.-H. Oxidation-bonded SiC membrane for microfiltration. *J. Eur. Ceram. Soc.* **2018**, *38*, 1711–1719. [CrossRef]

19. Guo, W.; Xiao, H.; Yao, X.; Liu, J.; Liang, J.; Gao, P.; Zeng, G. Tuning pore structure of corrosion resistant solid-state-sintered SiC porous ceramics by particle size distribution and phase transformation. *Mater. Des.* **2016**, *100*, 1–7. [CrossRef]
20. Luo, Z.-Y.; Han, W.; Yu, X.-J.; Ao, W.-Q.; Liu, K.-Q. In-situ reaction bonding to obtain porous SiC membrane supports with excellent mechanical and permeable performance. *Ceram. Int.* **2019**, *45*, 9007–9016. [CrossRef]
21. Chen, Y.; Li, S.; Luo, Y.; Xu, C. Fabrication of polycarbosilane and silicon oxycarbide microspheres with hierarchical morphology. *Solid State Sci.* **2011**, *13*, 1664–1667. [CrossRef]
22. Chen, M.; Shang, R.; Sberna, P.M.; Luiten-Olieman, M.W.; Rietveld, L.; Heijman, S.G. Highly permeable silicon carbide-alumina ultrafiltration membranes for oil-in-water filtration produced with low-pressure chemical vapor deposition. *Sep. Purif. Technol.* **2020**, *253*, 117496. [CrossRef]
23. Nagano, T.; Sato, K.; Kawahara, K. Gas Permeation Property of Silicon Carbide Membranes Synthesized by Counter-Diffusion Chemical Vapor Deposition. *Membranes* **2020**, *10*, 11. [CrossRef] [PubMed]
24. Poli, A.; Dagher, G.; Santos, A.F.; Baldoni-Andrey, P.; Jacob, M.; Batiot-Dupeyrat, C.; Teychené, B. Impact of C-CVD synthesis conditions on the hydraulic and electronic properties of SiC/CNTs nanocomposite microfiltration membranes. *Diam. Relat. Mater.* **2021**, *120*, 108611. [CrossRef]
25. Facciotti, M.; Boffa, V.; Magnacca, G.; Jørgensen, L.B.; Kristensen, P.K.; Farsi, A.; König, K.; Christensen, M.L.; Yue, Y. Deposition of thin ultrafiltration membranes on commercial SiC microfiltration tubes. *Ceram. Int.* **2014**, *40*, 3277–3285. [CrossRef]
26. Liang, D.; Huang, J.; Zhang, H.; Fu, H.; Zhang, Y.; Chen, H. Influencing factors on the performance of tubular ceramic membrane supports prepared by extrusion. *Ceram. Int.* **2021**, *47*, 10464–10477. [CrossRef]
27. Ojalvo, C.; Jiménez-Fuentes, M.; Zhang, W.; Guiberteau, F.; Candelario, V.M.; Ortiz, A.L. Fabrication of B4C ultrafiltration membranes on SiC supports. *J. Eur. Ceram. Soc.* **2022**, *42*, 3118–3126. [CrossRef]
28. Huang, Z.; Sun, W.; Wang, C.; Chen, C.; Huang, J.; Chen, S.; Hu, P. Recrystallization sintering and characterization of composite powders composed of two types of SiC with dissimilar particle sizes. *Int. J. Appl. Ceram. Technol.* **2022**, *19*, 1929–1938. [CrossRef]
29. Li, Y.; Wu, H.; Liu, X.; Huang, Z.; Jiang, D. Microstructures and properties of solid-state-sintered silicon carbide membrane supports. *Ceram. Int.* **2019**, *45*, 19888–19894. [CrossRef]
30. Petrus, M.; Wozniak, J.; Cygan, T.; Kostecki, M.; Olszyna, A. The effect of the morphology of carbon used as a sintering aid on the mechanical properties of silicon carbide. *Ceram. Int.* **2019**, *45*, 1820–1824. [CrossRef]
31. Li, S.; Luo, X.; Zhao, L.; Wei, C.; Gao, P.; Wang, P. Crack tolerant silicon carbide ceramics prepared by liquid-phase assisted oscillatory pressure sintering. *Ceram. Int.* **2020**, *46*, 18965–18969. [CrossRef]
32. Liu, G.; Dai, P.; Wang, Y.; Yang, J.; Zhang, Y. Fabrication of wood-like porous silicon carbide ceramics without templates. *J. Eur. Ceram. Soc.* **2011**, *31*, 847–854. [CrossRef]
33. Fraga, M.C.; Sanches, S.; Pereira, V.J.; Crespo, J.G.; Yuan, L.; Marcher, J.; de Yuso, M.V.M.; Rodríguez, C.; Benavente, J. Morphological, chemical surface and filtration characterization of a new silicon carbide membrane. *J. Eur. Ceram Soc.* **2017**, *37*, 899–905. [CrossRef]
34. Hotza, D.; Di Luccio, M.; Wilhelm, M.; Iwamoto, Y.; Bernard, S.; da Costa, J.C.D. Silicon carbide filters and porous membranes: A review of processing, properties, performance and application. *J. Membr. Sci.* **2020**, *610*, 118193. [CrossRef]
35. Fan, H.; Xiao, K.; Mu, S.; Zhou, Y.; Ma, J.; Wang, X.; Huang, X. Impact of membrane pore morphology on multi-cycle fouling and cleaning of hydrophobic and hydrophilic membranes during MBR operation. *J. Membr. Sci.* **2018**, *556*, 312–320. [CrossRef]
36. Park, D.J.; Jung, Y.I.; Kim, H.G.; Park, J.Y.; Koo, Y.H. Oxidation behavior of silicon carbide at 1200 °C in both air and water-vapor-rich environments. *Corros. Sci.* **2014**, *88*, 416–422. [CrossRef]
37. Chen, G.; Hong, D.; Xia, H.; Sun, W.; Shao, S.; Gong, B.; Wang, S.; Wu, J.; Wang, X.; Dai, Q. Amorphous and homogeneously Zr-doped MnOx with enhanced acid and redox properties for catalytic oxidation of 1,2-Dichloroethane. *Chem. Eng. J.* **2022**, *428*, 131067. [CrossRef]
38. Wiśniowska, J.; Zych, Ł.; Gubernat, A.; Mastalska-Popławska, J.; Jakubas, K.; Zientara, D.; Nocuń, M. Stabilisation, rheology and application of aqueous suspensions of oxidised vs. non-oxidised SiC powder. *Mater. Chem. Phys.* **2023**, *295*, 127153. [CrossRef]
39. Gao, X.; Wang, R.; Zhao, J.; Huang, J.; Gao, Y.; Liu, H. Influence of surface oxide layer of SiC powder on the rheological properties of its slurry. *Int. J. Appl. Ceram. Technol.* **2019**, *17*, 484–490. [CrossRef]
40. Zhao, L.; Jia, D.; Duan, X.; Yang, Z.; Zhou, Y. Oxidation of ZrC–30vol% SiC composite in air from low to ultrahigh temperature. *J. Eur. Ceram. Soc.* **2012**, *32*, 947–954. [CrossRef]
41. Zhou, C.L.; Liu, D.Z.; Zhi, W.; An, J.D.; Hu, P.; Han, W.B. Oxidation behaviour of C–SiC–ZrC composite. *Mater. Res. Innov.* **2015**, *19*, S1–S375. [CrossRef]
42. Remyamol, T.; Gopi, R.; Ajith, M.; Pant, B. Porous silicon carbide structures with anisotropic open porosity for high-temperature cycling applications. *J. Eur. Ceram. Soc.* **2020**, *41*, 1828–1833. [CrossRef]
43. Zhuang, L.; Fu, Q.; Tan, B.; Guo, Y.; Ren, Q.; Li, H.; Li, B.; Zhang, J. Ablation behaviour of C/C and C/C–ZrC–SiC composites with cone-shaped holes under an oxyacetylene flame. *Corros. Sci.* **2016**, *102*, 84–92. [CrossRef]
44. Kim, Y.; Kim, Y.; Seo, W. Processing and properties of silica-bonded porous nano-SiC ceramics with extremely low thermal conductivity. *J. Eur. Ceram Soc.* **2020**, *40*, 2623–2633. [CrossRef]
45. Abadikhah, H.; Wang, J.-W.; Xu, X.; Agathopoulos, S. SiO_2 nanoparticles modified Si_3N_4 hollow fiber membrane for efficient oily wastewater microfiltration. *J. Water Process. Eng.* **2019**, *29*, 100799. [CrossRef]

46. Li, S.; Wei, C.; Wang, P.; Gao, P.; Zhou, L.; Wen, G. Zirconia ultrafiltration membranes on silicon carbide substrate: Microstructure and water flux. *J. Eur. Ceram. Soc.* **2020**, *40*, 4290–4298. [CrossRef]
47. Gao, Y.; Hao, W.; Xu, G.; Wang, C.; Gu, X.; Zhao, P. Enhancement of super-hydrophilic/underwater super-oleophobic performance of ceramic membrane with TiO_2 nanowire array prepared via low temperature oxidation. *Ceram. Int.* **2022**, *48*, 9426–9433. [CrossRef]
48. Zhu, J.; Fan, Y.; Xu, N. Modified dip-coating method for preparation of pinhole-free ceramic membranes. *J. Membr. Sci.* **2011**, *367*, 14–20. [CrossRef]